2022 IEEE International Conference on Robotics and Automation (ICRA)
May 23-27, 2022. Philadelphia, PA, USA

Experimental Validation of the Usage of Kinematic Singularities to Produce Periodic High-Powered Motion

Chang Liu[1] and Mark Plecnik[2]

2022 IEEE International Conference on Robotics and Automation (ICRA) | 978-1-7281-9681-7/22/$31.00 ©2022 IEEE | DOI: 10.1109/ICRA46639.2022.9811546

Abstract— **This paper reports on preliminary experimental results of recently proposed mechanism kinematics for a legged robot. The proposed kinematics creates a mapping from a series-elastic actuator to a foot motion that includes a pair of singularities within a fully rotatable kinematic circuit. Such a circuit is less common and only possible with certain multi-loop linkages. A slice of the configuration space displaying series-elastic rotation versus linear foot motion presents a characteristic "S" shape, motivating the name S-curve kinematics. Our experimental results show that S-curve kinematics can enhance the energetic output of a series-elastic actuator in a hopping task versus the usage of a conventional rotary-to-linear mechanism. This is possible because S-curve kinematics enable elastic energy storage outside of stance that is released through a mechanical reflex. Compared to a conventional rotary-to-linear actuator, S-curve kinematics demonstrated up to a 4x increase in kinetic output.**

I. Introduction

This paper presents an experimental validation of proposed leg mechanism kinematics for increasing the energetic output of a series-elastic actuator (SEA). Such kinematics purposefully incorporate a specific arrangement of singularities between the rotation of the SEA and the translation of an output foot. Here singularities are defined as configuration points where the derivative of foot motion with respect to SEA rotation tends toward infinity. The target kinematic arrangement holds both singularities on a single kinematic circuit [1] that allows the SEA to fully rotate. It is more common that singularities with respect to an input rotation mark the global bounds of range of motion within a circuit. In this work, we highlight kinematics where singularities only mark these bounds in a narrow local region of a circuit which maintains unlimited rotation of the input SEA. Such an arrangement is only possible for certain multi-loop linkages. Following a simple input-output power balance, it can be shown that at configurations in the neighborhood of a singularity, small forces acting in the direction of foot motion multiply into large torques that act against the SEA. At a singularity exactly, the mechanism reacts to any applied SEA torque with an equal and opposite torque, even when no load is applied at the foot.

It is this feature of singularities that we exploit for an energetic advantage. SEAs are recognized for allowing transient energy storage in their elastic element during dynamic motions when they are commanded to quickly push an inertia [2], [3]. It is this inertial load acting through a mechanism which works against an SEA to build up energy in its elastic element. In the absence of such an inertial load, elastic storage is generally not possible except at a singularity. In the context of legged hopping, elastic storage is possible in stance phase when an SEA is working to accelerate inertia by pushing off the ground, and sizable storage is practically impossible during flight phase. However, when acting against a singularity, an SEA is still able to build up elastic energy during ballistic motion of the legged robot throughout flight.

It is advantageous that singularities enable an SEA to build up elastic energy in both stance phase and flight phase. In conventional singularity-free mechanisms, postive work done by actuators is relegated to energizing the system only during stance. Enabling the storage of elastic potential during flight phase can extend the energetic profile of a robotic leg roughly by a factor equal to the reciprocal of the duty factor. Airborne elastic gains may be dispensed at a high rate during a subsequent stance phase to convert this potential into kinetic energization of the center of mass.

The idea presented above assumes that elastic potential stored in flight will be dispensed during stance in a useful and lossless manner. This is easier said than done. The instantiation of the aforementioned singularities multi-functionally serve to provide a solution to this problem as well. As mentioned earlier, in the neighborhood of configurations around these singularities, a small force acting along the foot transforms into a large torque acting against the SEA. In other words, foot forces will dominate over SEA torque near these configurations. This instantiates a mechanical reflex whereby impacts with the ground function to advance the configuration out and away from the singular neighborhood into a regular region which is mechanically programmed to usefully dispense the elastic potential stored during flight. For example, in a hopping task, the configurations subsequent to the singular neighborhood comprise a straight line push-off motion. Since the proposed kinematic circuit fully rotates the SEA, subsequent to this push-off, the SEA reconfronts the same singularities in flight, enabling airborne energization for the next cycle.

This mechanical reflex improves the periodicity of motion in the absence of motor control. The utility of completely foregoing motor control is not an end in itself, but rather a means to off-load fast, low-level dynamics to natural mechanics. The timescale of said dynamics challenges the latency of a state machine control loop.

The kinematics described above are termed *S-curve* kine-

*This material is based upon work supported by the National Science Foundation under Grant Nos. CMMI-2041789 and CMMI-2144732.

[1]Chang Liu is a Graduate Student in the Department of Aerospace & Mechanical Engineering at the University of Notre Dame cliu23@nd.edu

[2]Mark Plecnik is an Assistant Professor in the Department of Aerospace & Mechanical Engineering at the University of Notre Dame plecnikmark@nd.edu

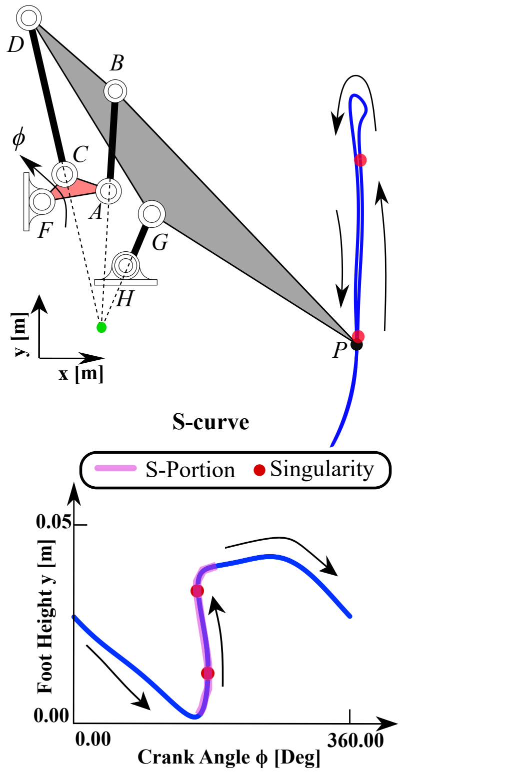

Fig. 1. Kinematic diagram of the S-curve mechanism. The S-curve refers to the "S" shape in the ϕ-y slice of the configuration space. Singularities are marked in both the task space and the configuration space. The mechanism is classified as a Stephenson II six-bar. For this type, the geometric condition of singularity is for links AB, CD, and GH to have a common intersection, marked in green above. S-curve kinematics can enhance the energetic output of a series-elastic actuator in a hopping task.

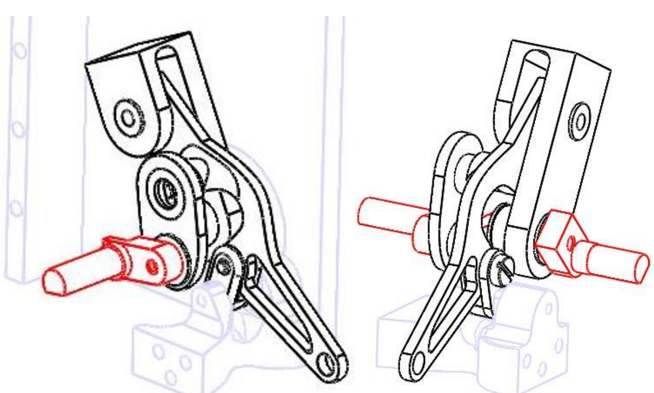

Fig. 2. The S-curve mechanism used in this paper. The input link is highlighted in red, the other moving links & joints are sketched in black. The ground link is printed lightly. Two different orientations are shown to illustrate the form of the assembly.

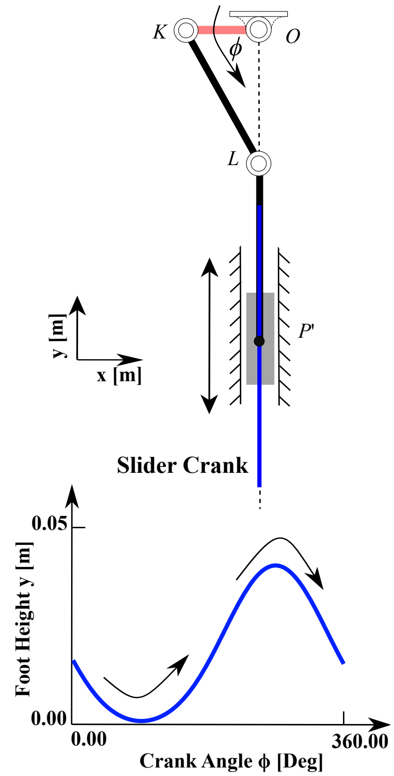

Fig. 3. Kinematic diagram of the slider-crank, a conventional rotary-to-linear linkage that serves as an experimental control where a stroke length similar to the approximate straight line of the S-curve mechanism, but has no singularities in its configuration space.

TABLE I

PIVOT LOCATIONS IN A REFERENCE CONFIGURATION FOR THE S-CURVE MECHANISM (FIG .1) AND THE SLIDER-CRANK MECHANISM (FIG.3).

Pivot	**Dimensions** (mm)	
	x	y
A	55.7229	−5.57402
B	−54.8716	8.62727
C	−62.1456	−3.58622
D	−67.5360	19.7554
F	−65.5195	−7.2907
G	−49.6631	−9.0554
H	−52.6500	−16.2000
P	−19.5040	−28.1592
K	−23.2410	0.0000
O	0.0000	0.0000
L	0.0000	−45.1718
P'	0.0000	−95.9718

matics due to the characteristic "S" shape that appears in their configuration space, see Fig. 1. In this paper, we employ a Stephenson II six-bar mechanism actuated at its ternary link. Its geometric condition for singularity is when links AB, CD, and GH share a common intersection point [4]. S-curve kinematics were first proposed in [5]. This work included several simulation studies for understanding how reshaping the "S" affects dynamic performance. These simulations were performed on *configuration spaces* rather than *mechanisms* themselves. What this means is that simulations were set up such that a DC motor model acted directly through a proposed configuration space to locomote a foot for a hopping motion without the need of a mechanism model. More technical information can be found in [6]. The contribution of this work is to propose a practical linkage design that exhibits S-curve kinematics, and the documentation of its construction and initial experimental validation. The initial experiment fixes the SEA-powered mechanism to a table upside down, then demonstrates repeated upward kicking of a mass constrained to a linear slide.

Various previous works have presented mechanisms capable of mechanically energizing a leg in the absence of ground contact using mechanical elements such as a bow and string [7], [8], a capstan [9], and a pneumatic mechanism [10]. In this work, we aim to achieve an energetic advantage through kinematically constrained input-output velocity ratios of a linkage. Manipulation of velocity ratios of a linkage has been used in the past to increase the energetic output of robot purely in stance phase [11], [12]. Related work looks to increase the energetic output of a two degree-of-freedom actuated mechanism by finding kinematics that evenly distribute the workload between actuators [13], and work well for multiple locomotion modes [14]. A unique feature of the S-curve mechanism presented in this work is its ability to create periodic motion without motor control. It has been shown that even the simplest hopping systems operating on open-loop control can easily lead to nonperiodic motions [15].

II. Overview of the S-Curve Mechanism

The six-bar linkage displayed in Fig. 1 exhibits S-curve kinematics. This may be verified by plotting the relationship between the rotation of its input link *ACF* and the translation of its output point *P* and noting a characteristic "S" shape. The six-bar linkage is of the Stephenson II-B type [16]. Its dimensions are displayed in Table I. It is actuated by a ternary link. The motor's axis aligns with *F*. The end-effector point, i.e. the *foot*, attaches to a floating ternary link. The foot traces an approximate straight line. The linkage of Fig. 1 is not meant to be a stand-alone leg mechanism. Instead, it would serve to actuate a thrust degree-of-freedom in a broader system. For example, additional mechanism may be designed to add a degree-of-freedom which angles the line-of-action and translates it to a more convenient location, see [17]. But for the basic experiments conducted in this paper, the linkage system of Fig. 1 suffices. A solid model embodiment of the kinematic diagram of Fig. 1 is shown in Fig. 2.

The functionality of the S-curve mechanism is described in context to the basic experiment performed in this paper, see Fig. 4. The mechanism was flipped upside down and fixed to a table. The motor was switched on, then a mass attached to a linear guideway was dropped onto the foot of the mechanism from above. After the motor switches on and before the mass makes contact, the motor drives the mechanism immediately into the singular neighborhood (i.e. the "S" portion of the configuration space between the two singularities) at which the mechanism stops. It worth noting that although theoretically two exact singularities exist in the

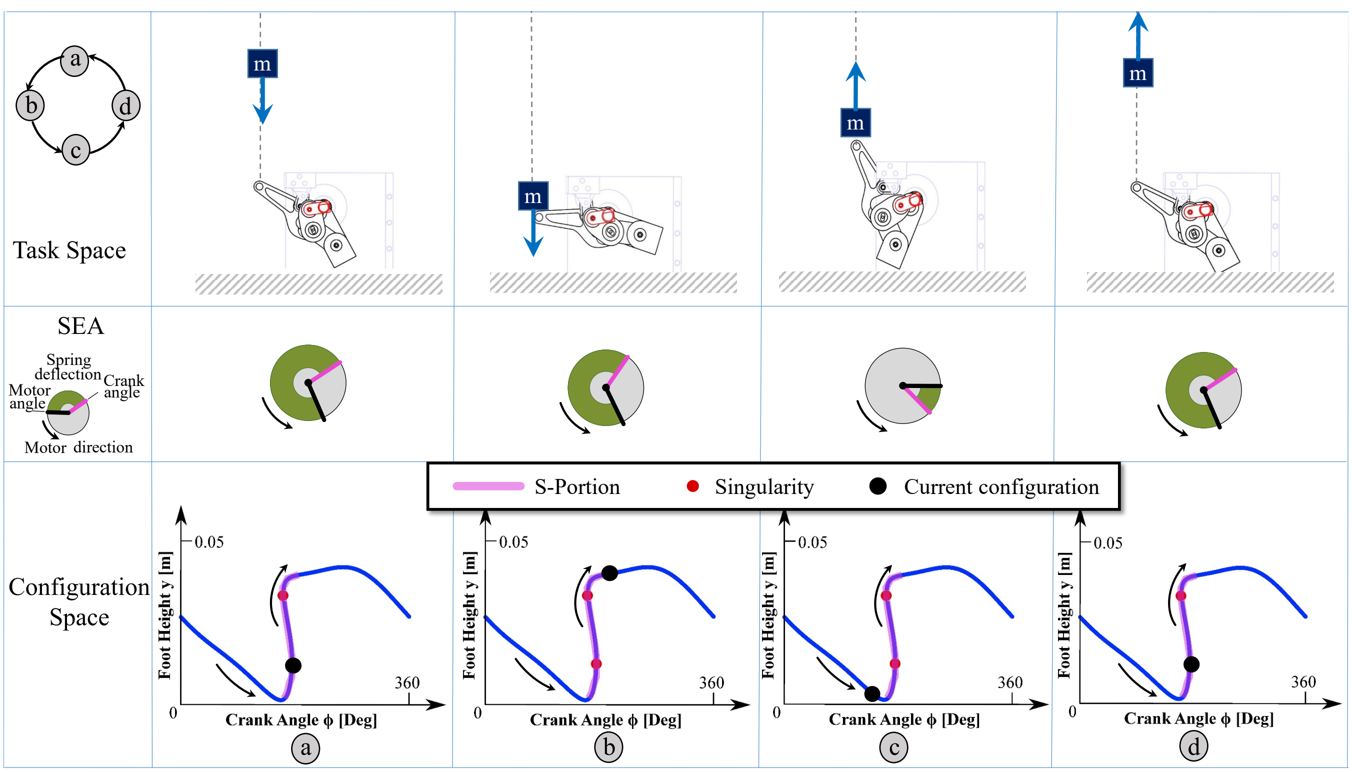

Fig. 4. A full motion cycle of the experiments with S-curve mechanics executed in this paper. The S-curve mechanism is mounted upside down and the mass *m* is attached to a vertical linear slide. ⓐ The mechanism engages into the singular region and builds elastic energy as the mass is airborne. ⓑ The mass makes contact with the mechanism's foot, advancing it out of the singular region. ⓒ Elastic power and motor power work together to accelerate the mass upwards. ⓓ While the mass is airborne, the mechanism advances into the singular region, and the cycle repeats. The cycle was found to work most repeatedly when the configuration in phase ⓐ set near the top of the singular region. Else, joint friction would occasionally inhibit advancement into ⓑ.

singular neighborhood, in practicality, the whole neighborhood functions as a singular region due to manufacturing inaccuracies and joint friction. Fig. 4a shows the mecha in the singular region with the motor powered on awa contact with the falling mass. In this configuration elastic element of the SEA is maximally strained. In Fig the contact force from impact with the mass advance mechanism out of the singular region. In Fig. 4c, the s energy stored in the SEA unloads into an upward motion, sending the mass out of contact. In Fig. 4d mechanism continues to cycle forward until it reache singular region, at which it charges the spring then a for next contact with the mass to continue the cycle.

To provide a point of comparison, this experiment also conducted on a conventional rotary-to-linear linkage. A slider-crank was selected as this conventional linkage, see Fig. 3. The slider-crank was dimensioned to have a stroke of length similar to the approximate straight line of the S-curve mechanism. The slider-crank has a fully rotatable and singularity-free configuration space, see Fig. 3. Its dimensional information is given in Table I.

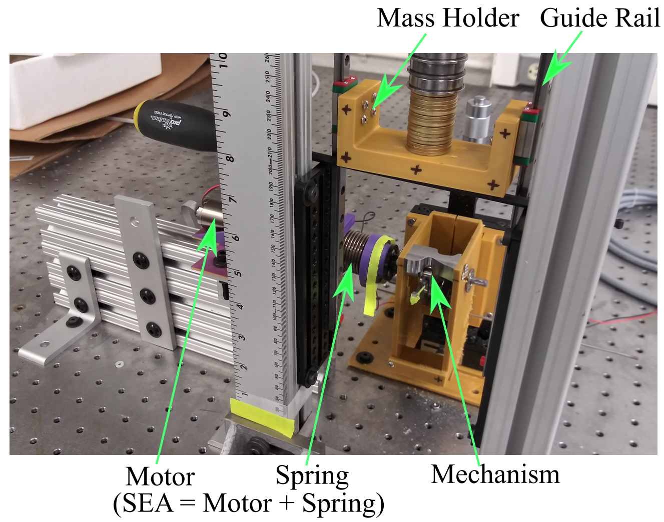

Fig. 7. The experimental set-up. The SEA and experimental mechanism were fixed upside down to a table. A mass was attached to a vertical linear guiderail overtop the mechanism.

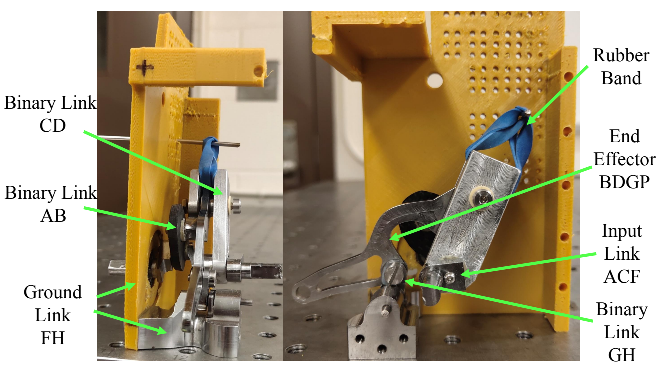

Fig. 5. Physical prototype of the S-curve mechanism.

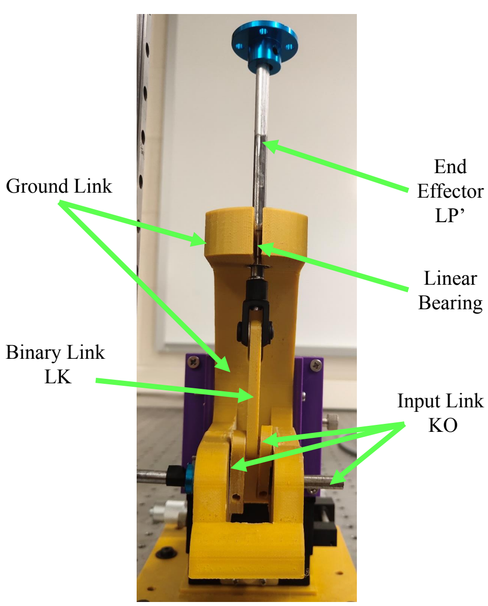

Fig. 6. Physical prototype of the slider-crank mechanism.

III. Methods

A. Fabrication

The S-curve mechanism shown in Fig. 1 was fabricated using a combination of materials and manufacturing techniques. The resulting prototype is shown in Fig. 5 with links labelled. Input link *ACF* took the most complicated form in order to avoid link interferences and aid in assembly. It was CNC machined out of 4140 steel as three separate parts that bolted together during assembly. Binary link *GH* and end-effector link *BDGP* were also CNC machined out of 4140 steel. Binary link *CD* took a larger form but sufficed to be CNC machined from 6061 aluminum. Binary link *AB* took a simpler form and so was conventionally machined from 5 mm thick carbon fiber sheet. Ground link FH, referred to as the *body*, comprised of two halves 3D printed with PLA rigidly bolted to a CNC machined part of 4140 steel. The steel portion of the body was necessary to withstand the loads at point H. All joints of the mechanism were accommodated with bushings or ball bearings as space allowed. Preliminary experiments revealed that the mechanism would set differently within the singular region under different dynamic loading conditions. To increase the repeatability of this set, a rubber band was added that connected the back of link *CD* to ground, which pulled the mechanism into a consistent position across operating conditions. The scale of the designed mechanism was chosen to accommodate off-the-shelf components, but biased toward the smaller side. Scaling down is possible but would be challenged by a limited selection of off-the-shelf components, an increased influence of friction, and a need for more precise manufacturing. Scaling up is possible but would be challenged by a greater influence of inertial forces.

The slider-crank mechanism shown in Fig. 3 was fabricated mostly from 3D printed components, as its links experienced smaller forces. Its ground link, input link *KO*, and binary link LK were 3D printed of PLA. Its end-effector link LP' served as the sliding member. It was fabricated from 6.35 mm aluminum tube that slid in a linear reciprocating ball bearing housed in the ground link. Link LP' connected to LK via a plastic clevis. An aluminum shaft coupler was fixed to its opposing end to provide a surface contact with the mass. The slider-crank was also outfitted with a combination of bushings and ball bearings.

B. Experiments

To evaluate the dynamic performance of the proposed S-curve mechanics, an experimental set-up was devised for mounting the S-curve mechanism and slider-crank (the experimental control), see Fig. 7. Each mechanism was fixtured upside down so that its end-effector kicks upward a mass mounted to a vertical guide rail. The mechanisms were powered by a fixed SEA. The reasoning of this inverted experiment was to (1) isolate S-curve mechanics for evaluation in the absence of confounding factors such as lateral forces, (2) create an environment that mimics the continuous and periodic nature of hopping, and (3) allow for an easily measurable performance metric: kick height.

Both the S-curve mechanism and the slider-crank were powered by the same SEA. The SEA was formed by coupling a Maxon DCX26L motor with a 0.29 Nm/rad spring (McMaster-Carr, part no. 9271K986). The motor was controlled by Maxon's EPOS Studio software running torque control through an EPOS4 controller. For all trials, the target torque value was set at 2.2 Nm, which was only actually reached for the S-curve mechanism. The mass attached to the linear guideway was varied for three discrete values: light (307g), medium (361g), and heavy (443g). For each experimental mechanism, we conducted five trials for each mass value. A trial consisted of switching the motor on, then dropping the mass onto the mechanism. It is worth noting that the S-curve mechanism was assembled with a rubber band installed (Fig. 5). This modification was made after noting during preliminary tests that the mechanism would settle in the singular region in a larger than intended range of configurations. The rubber band acted to pull the mechanism into a consistent position for a wide array of dynamic loading conditions. It was set to configure the mechanism close to exiting the singular region. This was decided in order to lower the magnitude of the impact force required to advance the mechanism. Theoretically, this required magnitude should be quite small. In reality, friction at each of the joints plays a role to increase the required impact magnitude. Additionally, the S-curve mechanism and slider-crank possessed different contact surfaces that interacted with the plastic mass holder. The S-curve mechanism had a small steel tip, while the slider-crank had a larger aluminum area.

Motor torque was recorded with Maxon's software as *percentage values* (originally derived from current values). These percentages values were correlated to Nm through calibration testing performed on the side to provide an estimate of motor torque. Torque values were recorded for five seconds of each trial at a sampling rate of 100 Hz. Torque values were used to estimate spring deflection and elastic energy storage assuming Hooke's law (k = 0.29 Nm/rad). Kick height was recorded by a video camera with a frame rate of 30 fps, and was later measured with video tracking software [18]. In total, data was collected for 30 experiments, 15 for the S-curve mechanism and 15 for the experimental control slider-crank mechanism.

IV. Results and Discussion

Figure 8 displays kick height and spring energy storage plotted over time for the S-curve mechanism and the slider-crank for all three masses. For the heavy mass, average kick height of the S-curve mechanism was 0.215 m, while the slider-crank kicked the mass up to 0.069 m on average (factor of 3.1). For the medium mass, the S-curve kick height averaged 0.220 m, whereas slider-crank averaged 0.080 m (factor of 2.8). For the light mass, average kick height of the S-curve was 0.333 m, and the slider-crank kicked the mass up to 0.081 m on average (factor of 4.1). For the S-curve mechanism, the energy stored in the spring was estimated at 8.4 J after each impact, and that energy is released upon

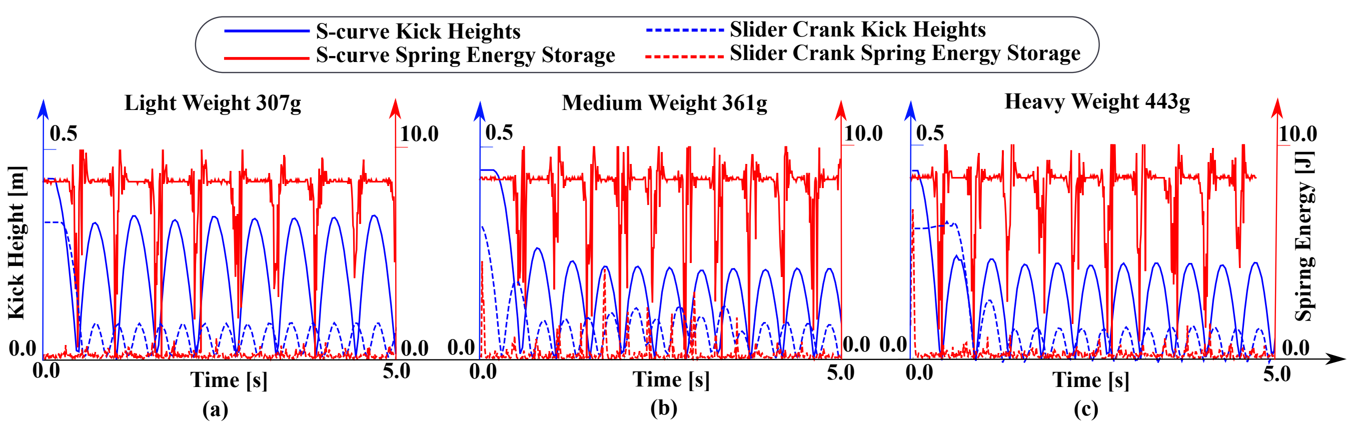

Fig. 8. Selected results for three different masses the mechanisms kicked in the experiments. Both kick height and spring energy storage is recorded and plotted. The S-curve mechanism demonstrates up to a 4x increase in kinetic output. Trials with medium weight are performed with deformed end effector link (Fig. 9).

the subsequent impact and transferred into kinetic energy of the mass. This is in sharp contrast to the slider-crank mechanism, where the spring energy storage is nearly zero at all times. Moreover, even though the motor is only running with a simple fixed torque set point, the S-curve mechanism produces high-powered motion that is near periodic, storing energy at the singular region as the mass is in the air, and releasing stored energy upon impact for useful kinetics of the mass, then continuing the cycle. With the slider-crank mechanism, on the other hand, the impact configuration is random, and the energy storage within the SEA is essentially zero. The nonperiodic motion of the slider-crank is most visible in Fig. 8b.

Even though our proposed S-curve mechanism demonstrated superior performance over the conventional slider-crank mechanism, it seemed to exhibit large energy losses. For example, in trials with medium mass, the 8.4 J of the spring potential was depleted after impact, but only $\approx$1 Joule is transferred into kinetic energy (Fig. 8b). We hypothesize that multiple factors could contribute to this energy loss. This would include damping losses such as: motor and spring damping, link deflection (including plastic deformation), joint friction, unintended lateral friction due to out-of-plane link deflection and joint slop, and losses from friction in the linear guideway. Engineering activities to mitigate some of these losses include revising link geometries to improve stiffness and eliminate plastic deformation; and revising bearing selection to reduce friction and slop.

An additional observation was that the kick heights of the S-curve mechanism were very similar for medium and heavy masses. One would assume that the heavier masses would result in lower kick heights. We conject that these results were due to the order in which tests were conducted, that is: five trials with the light mass, five trials with the heavy mass, and five trials with the medium mass. At the conclusion of testing, at least one component, the end-effector link, was seen to have plastically deformed (Fig. 9).

We also comment on the existence *double contact phases*. By this we refer to instances when immediately after impact the mass holder would experience a very short airborne phase

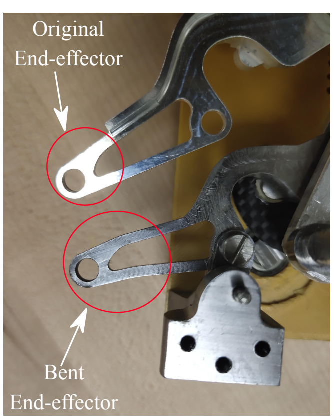

Fig. 9. The bent end-effector due to repeated kicking tasks versus the original end-effector link.

($<$ 10 ms), then re-make contact with the mechanism. We surmise these double contact phases had negative consequences on the usage of spring energy for the proceeding kick-off motion. Their exact cause should be studied further, but intuitively should be related to an underdamped condition set up by the current configuration's mechanical advantage and the series elastic actuator at the time of impact. Re-designing the shape and material of contact points of the end-effector link could potentially remove *double contact phases*.

Another issue was the presence of joint slop, which lead to kinematic inaccuracies and extra small motions. This could lead to undesired "circuit jumping". Following the definition of a kinematic circuit given in [1], this is when two distinct, disconnected circuits lie close enough in proximity to each other (in the configuration space), that a small amount of joint slop provides enough clear to jump the divide from one circuit to the other.

V. Conclusion

In this paper, we presented an experimental validation of recently proposed S-curve kinematics that aim to enable high-powered, periodic motions, with utility for legged robots. The proposed kinematics generates a mapping from an SEA to a foot motion with a pair of kinematic singularities that live on a fully rotatable kinematic circuit. Our experiments suggest that this mechanism is able to enhance the energetic output of an SEA by exploiting the airborne phase in a hopping motion through charging the on-board spring of the SEA while the mechanism is at a kinematic singularity. We compare our proposed S-curve kinematics to a conventional rotary-to-linear mechanism, and our results suggests that S-curve mechanics exhibits up to a 4x increase in kinetic output. Several potential issues related to energy losses and kinematic inaccuracies were identified.

Acknowledgment

This material is based upon work supported by the National Science Foundation under Grant Nos. CMMI-2041789 and CMMI-2144732.

References

[1] T. R. Chase and J. A. Mirth, "Circuits and Branches of Single-Degree-of-Freedom Planar Linkages," *Journal of Mechanical Design*, vol. 115, no. 2, pp. 223–230, June 1993.

[2] D. Paluska and H. Herr, "The effect of series elasticity on actuator power and work output: Implications for robotic and prosthetic joint design," *Robotics and Autonomous Systems*, vol. 54, no. 8, pp. 667–673, Aug. 2006.

[3] J. Hurst, A. Rizzi, and D. Hobbelen, "Series elastic actuation: Potential and pitfalls," in *International Conference on Climbing and Walking Robots*, 2004.

[4] C. Gosselin, "Kinematic analysis, optimization and programming of parallel robotic manipulators," 1988.

[5] C. Liu and M. Plecnik, "The usage of kinematic singularities to produce periodic high-powered locomotion," in *2021 IEEE/RSJ International Conference on Intelligent Robots and Systems (IROS)*. IEEE, pp. 909–915.

[6] ——, "Evaluating plane curves as constraints for locomotion on uneven terrain," in *International Design Engineering Technical Conferences and Computers and Information in Engineering Conference*, vol. 83990. American Society of Mechanical Engineers, 2020, p. V010T10A030.

[7] B. Brown and G. Zeglin, "The bow leg hopping robot," in *Proceedings. 1998 IEEE International Conference on Robotics and Automation (Cat. No.98CH36146)*, vol. 1, May 1998, pp. 781–786 vol.1.
[8] G. Zeglin, "The Bow Leg Hopping Robot," Ph.D. dissertation, Carnegie Mellon University, Pittsburgh, Pennsylvania, 1999.
[9] J. G. Nichol, S. P. Singh, K. J. Waldron, L. R. Palmer, and D. E. Orin, "System Design of a Quadrupedal Galloping Machine," *The International Journal of Robotics Research*, vol. 23, no. 10-11, pp. 1013–1027, Oct. 2004.
[10] J. Estremera and K. J. Waldron, "Thrust Control, Stabilization and Energetics of a Quadruped Running Robot," *The International Journal of Robotics Research*, vol. 27, no. 10, pp. 1135–1151, Oct. 2008.
[11] M. M. Plecnik, D. W. Haldane, J. K. Yim, and R. S. Fearing, "Design Exploration and Kinematic Tuning of a Power Modulating Jumping Monopod," *Journal of Mechanisms and Robotics*, vol. 9, no. 1, Feb. 2017.
[12] D. W. Haldane, M. M. Plecnik, J. K. Yim, and R. S. Fearing, "Robotic vertical jumping agility via series-elastic power modulation," *Science Robotics*, vol. 1, no. 1, p. eaag2048, Dec. 2016.
[13] J. M. Brown, J. L. Pusey, and J. E. Clark, "Design methodology of linkage morphology for high speed locomotion," in *2017 IEEE International Conference on Robotics and Biomimetics (ROBIO)*, Dec. 2017, pp. 730–736.
[14] D. J. Blackman, J. V. Nicholson, J. L. Pusey, M. P. Austin, C. Young, J. M. Brown, and J. E. Clark, "Leg design for running and jumping dynamics," in *2017 IEEE International Conference on Robotics and Biomimetics (ROBIO)*, Dec. 2017, pp. 2617–2623.
[15] J. G. Cham and M. R. Cutkosky, "Dynamic Stability of Open-Loop Hopping," *Journal of Dynamic Systems, Measurement, and Control*, vol. 129, no. 3, pp. 275–284, May 2007.
[16] A. Baskar and M. Plecnik, "Synthesis of Six-bar Timed Curve Generators of Stephenson-type Using Random Monodromy Loops," *Journal of Mechanisms and Robotics*, vol. 13, no. 1, 2020.
[17] A. Baskar, C. Liu, M. Plecnik, and J. D. Hauenstein, "Designing rotary linkages for polar motions," in *2021 IEEE/RSJ International Conference on Intelligent Robots and Systems (IROS)*. IEEE, pp. 1384–1391.
[18] D. Brown, "Tracker Video Analysis Software," www.physlets.org/tracker/.